Journal of Marine Research, 43, 553–579, 1985

A zero potential vorticity model of the North Brazilian Coastal Current

by G. T. Csanady[1]

ABSTRACT

The North Brazilian Coastal Current (NBCC) is idealized as an inertial, surface layer jet of equatorial origin, intruding along the coast into a northern water mass of constant, positive potential vorticity. Dissipation is accounted for by supposing that some equatorial water leaks out in the northwest corner of the intrusion. The problem is closed by adopting the free streamline boundary condition (between the northern and equatorial water masses) of continuous layer depth and velocity.

Calculations are made for flow (intruding and return) supposed parallel to the coast; this approximation is verified à posteriori. The results show a narrow intrusion region along the coast, equatorial fluid flowing northwestward next to the coast, peeling off and returning along the boundary streamline. When no leakage is postulated, the northern limit of the intrusion becomes a stagnation point where the coast and the boundary streamline meet. With substantial leakage postulated, the flow chokes at some limiting latitude, where the inviscid inertial model breaks down. However, a realistic intrusion-return flow pattern is calculated south of the choking latitude for a number of different illustrative cases. The key control parameter is the potential vorticity of the northern water mass, or in a nondimensional form, the ratio of the rest-depths, at a given latitude, of the equatorial and northern water masses.

The model accounts for a number of observed facets of NBCC behavior, notably its seasonal cycle, magnitude of the transports, intrusive and return flow.

1. Introduction

A boundary current flows northwestward along the edge of the continental shelf off the north coast of Brazil. In a discussion tracing the origin and fate of water masses within this current, Metcalf (1968) suggested that a distinction be made between a southeastern portion, which he called the North Brazilian Coastal Current, NBCC, and a northwestern portion, known historically as the Guiana Current. The discontinuity in subsurface oxygen content, identified by Metcalf as separating the two sections of the current, occurs between 8–9N at distances of 300–400 km from the coast (covered by Metcalf's hydrographic sections), i.e., well beyond the edge of the 150 km or so wide continental shelf. For later discussion it is also relevant to note that the sections showing the discontinuity were taken in October to December.

1. Woods Hole Oceanographic Institution, Woods Hole, Massachusetts, 02543, U.S.A.

On the basis of this and other studies carried out in the late sixties (Metcalf and Stalcup, 1967; Ryther *et al.*, 1967; and Cochrane, 1969), Metcalf suggested that the NBCC turns offshore a few degrees north of the equator, turns back upon itself, and forms the Equatorial Undercurrent. Because the surface 100 meters or so of the current are 26–27°C warm this cannot apply to all of the northward flowing water: however, the surface layer turning offshore could well end up in the North Equatorial Counter Current (NECC), and eventually flow eastward at latitudes between 3 and 10N.

Metcalf (1968) also implied that the NBCC and Guiana Currents are entirely distinct, the latter being formed from an inflow of the North Equatorial Current. This is difficult to reconcile with a considerable body of evidence establishing that the Guiana Current transports Amazon River water into the Caribbean (Ryther *et al.*, 1967; Steven and Brooks, 1972; Froehlich *et al.*, 1978; Kidd and Sander, 1979; Borstad, 1982). The Amazon River is a very large source of freshwater (about 0.2×10^6 m^3 s^{-1}) which depresses the salinity of a large region of the western tropical North Atlantic: Ryther *et al.* (1967) speak of a "million square miles" being so affected. However, excepting some shallow lenses of low salinity water occasionally found floating offshore, the salinity depression is only of order 1‰, requiring a current with transport of order 10^7 m^3 s^{-1} to carry it all away. Currents on the continental shelf are too weak to account for more than a small fraction of the freshwater transport, and there can be little doubt that it is the NBCC-Guiana Current system that transports the Amazon water northwestward, most of it perhaps into the NECC, but a great deal further westward to the longitude of Barbados, 60W, and beyond.

The seeming conflict may be resolved by supposing that only part of the surface layer NBCC turns offshore to form the NECC, with a portion (of order 10^7 m^3 s^{-1} transport) continuing northwestward as part of the Guiana Current. A recent detailed study of currents off the continental shelf between 2–7N by Flagg and McDowell (1984) showed strong surface currents, northwestward as well as southeastward return flow, extending to some 400 km seaward from the edge of the continental shelf. Metcalf's studies were based on evidence collected within the outer half of this current system, so that all the above quoted facts are accounted for if one supposes some and only some outer streamlines to turn offshore at latitudes up to 9N.

Considerable support is given this idea by Richardson and McKee's (1984) study of surface currents in the equatorial Atlantic based on ship drift observations. An earlier study of Molinari (1983), using drifting buoys, gave similar results in less detail. The ship drift maps of Richardson and McKee show the outer ⅔ or so of the streamlines of the NBCC turning offshore and forming the NECC between July and December. In these months the total westward transport of warm surface water by the South Equatorial Current (SEC) may be estimated to be of order 30×10^6 m^3 s^{-1}, on the basis of the ship drift map and an assumed depth of 100 m. The same rough estimate follows from cross sections shown by Philander and Düing (1979). The warm SEC

waters end up in the surface layer of the NBCC, continuing on a northwestward course up to the bifurcation of this surface current into a coastal Guiana Current and a retroflecting NECC. The eastward transport of the latter was estimated by Cochrane (quoted by Philander and Düing, 1979) at 17×10^6 m^3 s^{-1}, or roughly 60% of the total estimated NBCC transport.

In the months January–July the transport of the SEC reduces considerably, to some 10^7 m^3 s^{-1}, estimated again on the basis of Richardson and McKee's maps. During these months no NECC forms, the westward transport of warm SEC waters continuing as northwestward flow in the NBCC and then in the Guiana Current.

In another important recent study comparing the NBCC and the Somali Current, Bruce (1984) cites further evidence for the continuity of the inner (nearshore) streamlines of the surface NBCC, and the seasonal turnoff of outer streamlines. He also mentions the frequent detection of warm core eddies (or meanders) by ships using the "western sea lane," a shore-parallel lane located about 300–400 km off the edge of the North Brazilian continental shelf. The illustrations of Bruce show that these eddies have a typical diameter decreasing with latitude from about 400 km at 4N to 200 km at 8N. The center depth of the pycnocline in the eddies is between 150–180 m. The surface of the eddies is often covered by a thin low salinity lens, evidently of Amazonian origin, as reported eariler by Hurlburt and Corwin (1969).

Bruce (1984) also draws attention to the upwelling along the inshore edge of the NBCC, which is weaker than in the Somali Current, but consistently reported, see also Gibbs (1980). Although most of the Somali Current is thought to turn offshore, there is some evidence for "leakage" also from this current northward along the coast, but of a much smaller quantity of water than in the NBCC-Guiana Current system.

A detailed scrutiny of the observations of Flagg and McDowell sheds further light on the behavior of the warm layer off the North Brazilian coast near 5N. Figure 1 shows the density distribution in a cross section extending from 4°30′N to 7N. The warm layer ($\sigma_t \leq 25.0$) has a bowl-like shape suggesting northwestward flow at the coast, return flow offshore. Flagg and McDowell estimate warm layer volume transports of 16.5×10^6 m^3 s^{-1} northwestward, 14.9×10^6 m^3 s^{-1} southeastward, mostly on the basis of directly observed current profiles (which agree fairly well with geostrophic velocities). The return flow, however, is not confined to the intruding (equatorial) water mass: this may be seen on the horizontal distribution of potential vorticity, Figure 2. The intruding water mass is characterized by low potential vorticity. A different, relatively high potential vorticity water mass flows southeastward along the outer edge of the equatorial intrusion. Comparison of the two figures shows that roughly half the southeastward flowing water mass is of northern origin. The mass balance of the equatorial water mass is then, at this section, about 17×10^6 m^3 s^{-1} northwestward transport, 7×10^6 m^3 s^{-1} return transport, i.e., about 10^7 m^3 s^{-1} net northwestward transport.

Given the limited resolution of the observations, the potential vorticity distribution

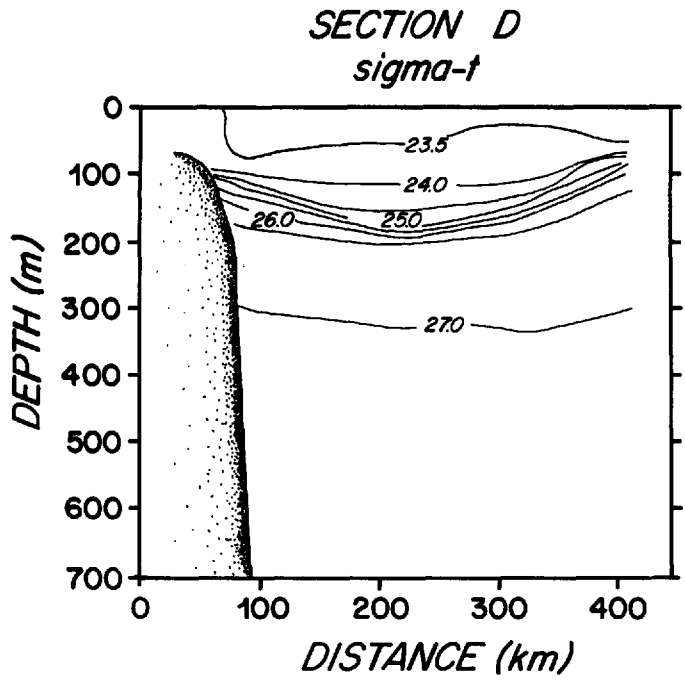

Figure 1. Density (σ_t) distribution in transect "D" of Flagg and McDowell (1984), between 4°28′N, 51W and 7°8′N, 48W, which was the northwestern limit of their study.

estimated by Flagg and McDowell is rather noisy. Figure 3 shows this distribution section by section, or rather by observed section-pair (attributed to the section halfway in between), because spatial gradients are involved. The core of the intruding water mass has approximately zero potential vorticity within the accuracy of these observations, although there is a suggestion in the cross sections that the difference in potential vorticity is eroding in the direction of flow. The displaced northern water mass has potential vorticity $(f + \zeta)/h$ of about 3×10^{-7} m^{-1} s^{-1}. The subsurface layer ($\sigma_t > 25.0$) was found to turn off at a lower latitude than the surface layer, complicating the pressure field somewhat. The observations were taken in December, i.e., in a period when Richardson and McKee's ship drift studies showed substantial flow from the NBCC into the NECC, although at a rate somewhat below the seasonal peak in September.

The behavior of the warm equatorial surface layer is of considerable interest also from the point of view of global heat balance, on account of the likely importance of equatorial upwelling and warm water mass formation (Csanady, 1984). The observations of the NBCC suggest that an important control mechanism may operate at the western boundary of an equatorial ocean, where the westward drift of the warm surface layer runs into a coast. Inertial effects may limit poleward heat and mass transport by the boundary current to some ceiling set perhaps by an interplay between

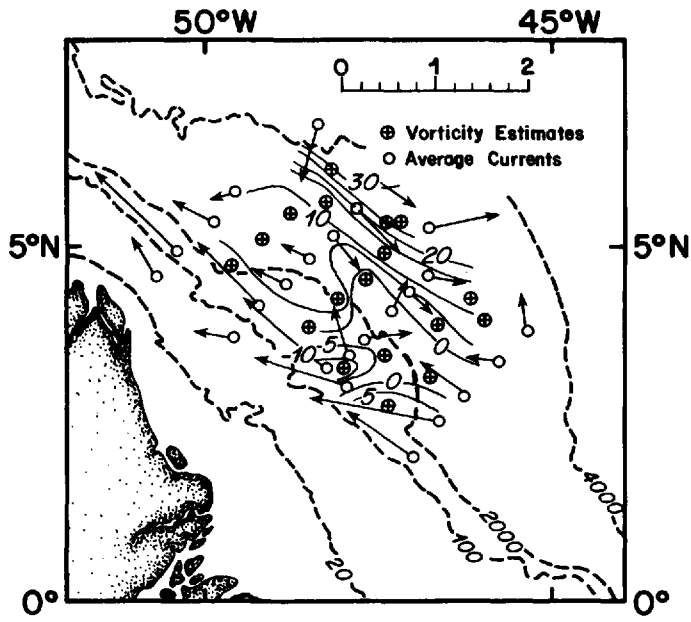

Figure 2. Horizontal distribution of potential vorticity (contours of 10^{-8} m^{-1} s^{-1}). Arrows show velocity vectors, scale at top right. Redrawn from Flagg and McDowell (1984).

earth rotation and sphericity, and such properties of the warm layer as depth and density defect. The objective of the present paper is to explore this possibility, and to account for those facets of NBCC behavior which are inertially controlled.

A reasonable idealization suggested by the distribution of potential vorticity is that a zero potential vorticity, inertial, surface layer jet of equatorial origin intrudes northwestward along the coast, and displaces a northern water mass of the same density, but of moderately high positive potential vorticity. This is similar to the idealization adopted by Anderson and Moore (1979) in their model of the Somali Current, except that Anderson and Moore did not consider the properties of the water masses with which the Somali Current comes into contact. The surface layer jet was supposed to ride over a stagnant deepwater mass. The latter hypothesis will be retained here for simplicity, even though this ignores some potentially important complications associated with the behavior of the intermediate density water mass of the NBCC (σ_t = 25–27) which turns off at a low latitude and ends up in the Equatorial Undercurrent.

2. Governing equations

As Figure 2 illustrates, the surface layer of the NBCC has potential vorticity significantly less than the water it displaces, but not significantly different from zero. The intrusive water mass displaces water of higher potential vorticity, (which will here

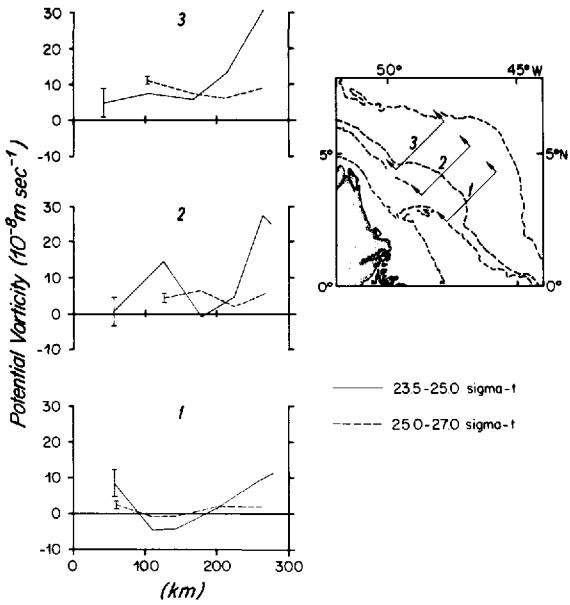

Figure 3. Potential vorticity in three sections mid-way between transects, in units of 10^{-8} m^{-1} s^{-1}. Courtesy of C. N. Flagg.

be supposed constant) but of the same density. Figure 4 illustrates schematically a two-layer idealization of the "equatorial" intrusion above the pycnocline, in contact with shelf waters and with a higher potential vorticity "northern" water mass offshore. The shelf water boundary will be supposed rigid, and replaced by a wall.

The coast and isobaths will be taken to enclose a constant angle ϕ against the equator (Fig. 5), coordinates x, y being chosen across and along isobaths. In a cross

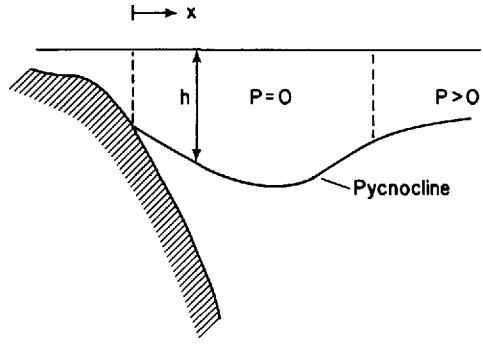

Figure 4. Schematic illustration of zero potential vorticity intrusion along the coast ($P = 0$), flanked by a northern water mass of the same, surface layer, density.

section (y = const) the Coriolis parameter varies as

$$f = f_o + \beta x \qquad f_o = \beta y \tan \phi \tag{1}$$

where $\beta = \beta_c \cos \phi$ is effective beta, with β_c the conventional value of $R^{-1}\partial f/\partial \lambda$, λ latitude, R earth radius. For the North Brazil coast, $\phi \simeq 40°$ and $\beta = 1.7 \times 10^{-11}$ m^{-1} s^{-1}. The value of the Coriolis parameter at the coast, f_o, is proportional to distance along the coast from the equator.

For a layer of fluid of depth h and of a constant proportionate density defect ϵ, lying over a deep, stagnant water mass of reference density ρ_o, the hydrostatic equation, continuity and equation of motion for the horizontal velocity vector $\mathbf{q}$ may be written

$$\begin{aligned} \frac{p}{\rho_o} &= \epsilon g h \\ \frac{\partial h}{\partial t} + \nabla \cdot (h\mathbf{q}) &= 0 \\ \frac{\partial \mathbf{q}}{\partial t} - \mathbf{q} \times \zeta = -\frac{1}{\rho_o}\nabla p - \frac{1}{2}\nabla q^2 &+ \mathbf{F} + \mathbf{q} \times f\mathbf{k} \end{aligned} \tag{2}$$

where $\zeta = \nabla \times \mathbf{q}$ is vorticity, a vertical vector, $\mathbf{F}$ an unspecified body force—such as friction or wind stress force distributed over layer depth —f is Coriolis parameter and $\mathbf{k}$ the vertical unit vector. Eqs. (2) are akin to those governing the flow of a compressible fluid in two dimensions, if h is thought of as analogous to density, and the hydrostatic equation to the equation of state.

An alternative way to express the above vector equations is in a so-called intrinsic form, with the velocity vector specified by its magnitude q and orientation angle θ (Fig. 6), and as functions of the "natural" coordinates s, n, parallel and perpendicular respectively to the velocity vector (see e.g., Woods, 1961):

$$\begin{aligned} \frac{\partial q}{\partial t} &= -\frac{\partial B}{\partial s} + F \\ \frac{\partial \theta}{\partial t} &= -(f + \zeta) - \frac{1}{q}\frac{\partial B}{\partial n} \\ \frac{\partial h}{\partial t} + hq\frac{\partial \theta}{\partial n} &+ \frac{\partial}{\partial s}(hq) = 0 \\ B &= \epsilon g h + \frac{1}{2}q^2 \\ \zeta &= q\frac{\partial \theta}{\partial s} - \frac{\partial q}{\partial n} \end{aligned} \tag{3}$$

where B is the Bernoulli function, and the external force is only indicated in the streamwise momentum equation. The first three of these equations give the rates of

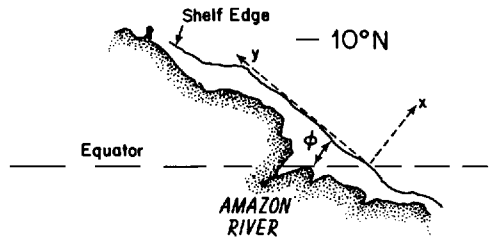

Figure 5. Orientation of coordinate system used in the parallel flow model.

change of the three dependent variables, q, θ and h in terms of various functions of the same dependent variables, including derivatives with respect to the independent variables s and n. The last two equations merely state definitions.

In the problems to be discussed below it is reasonable to regard the mean flow as steady. However, it is not quite realistic to neglect fluctuating motions altogether, because they may give rise to significant Reynolds stress (e.g., radiation stress associated with Rossby waves). Within a narrow boundary current the horizontal divergence of the Reynolds stress could conceivably become important, especially in the streamwise force balance which is more delicate than the quasi-geostrophic cross-stream balance. In applying Eqs. (3) to steady flow the external force F should be supposed to include any such Reynolds' stress divergence.

To minimize complexity, the external force F will nevertheless be neglected in the actual model calculations below, as in earlier inertial jet models. This does not yield a

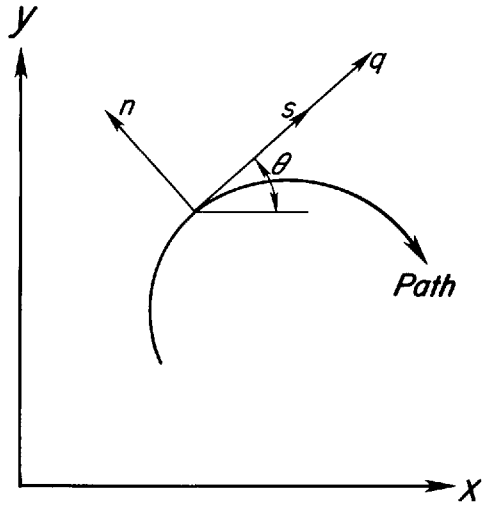

Figure 6. Intrinsic coordinates parallel and perpendicular to velocity vector of magnitude q, orientation angle θ.

completely accurate representation of the behavior of the intruding NBCC water mass, which exhibits a slow increase of the Bernoulli function northwestward. However, there is also a slow streamwise increase in potential vorticity (Fig. 3 above) with effects on the flow of the same order as the increase in the Bernoulli function, the consideration of which would unduly complicate the problem. The overidealizations should be kept in mind in interpreting the results.

For the postulated steady flow it is useful to introduce a transport stream function:

$$\begin{aligned} \frac{\partial \psi}{\partial n} &= hq \\ \frac{\partial \psi}{\partial s} &= 0. \end{aligned} \tag{4}$$

This function may be used to recalibrate the n axis and write Eqs. (3) as:

$$\begin{aligned} \frac{\partial \mathrm{B}}{\partial s} &= F \\ \frac{\partial \mathrm{B}}{\partial \psi} &= -\frac{f+\zeta}{h} \\ \frac{\partial \theta}{\partial \psi} &= \frac{\partial}{\partial s}\left(\frac{1}{hq}\right). \end{aligned} \tag{5}$$

With $F = 0$, the first two of these equations have been used in inertial jet and rotating fluid hydraulics problems a number of times, e.g., by Charney (1955), Gill (1977), and Anderson and Moore (1979). The third of (5) is sometimes forgotten: it expresses the kinematic necessity for streamlines to diverge (converge) with decreasing (increasing) transport hq.

Eqs. (5) are again a set of three, for the dependent variables q, θ and h, on a (s, ψ) grid. A solution describes a pattern of steady flow, and may be found e.g., by relaxation methods. In the special case of $F = 0$ the Bernoulli function and the potential vorticity, $(f + \zeta)/h$, are both constant along each streamline. When, in addition, all streamlines originate in a region where the potential vorticity vanishes, the equations reduce to:

$$\begin{aligned} h &= H - \frac{q^2}{2\epsilon g} \\ q\frac{\partial \theta}{\partial s} - hq\frac{\partial q}{\partial \psi} &= -f \\ \frac{\partial \theta}{\partial \psi} &= \frac{\partial}{\partial s}\left(\frac{1}{hq}\right) \end{aligned} \tag{5a}$$

with H the "rest-depth" of the top layer, which is prescribed.

3. Boundary conditions

The normal inviscid boundary condition is that solid boundaries constitute streamlines: this is readily applied at the coast or, in this case, at the edge of the continental shelf. However, the essence of the present problem is that one fluid mass intrudes into another, and displaces the latter, analogous to a free jet of air exhausting into a still medium. This gives rise to a free streamline boundary value problem, notorious for its difficulty, see e.g., Birkhoff and Zarantonello, (1957) or Woods (1961). In some such problems (of Helmholtz flow, as it is known in classical fluid mechanics) the pressure on the free streamline is prescribed as a boundary condition. The shape of the free streamline may then be calculated together with other characteristics of the flow. In many other cases, however, only the continuity of pressure across the free streamlines can be stipulated, so that some further condition is necessary to close the problem. Highly artificial conditions have at times been used in aerodynamics, see some examples quoted by Woods (1961).

The problem here under consideration belongs to a sub-branch of fluid mechanics sometimes described as rotating fluid hydraulics (Gill, 1977; Shen, 1981). As Shen emphasizes, the choice of boundary conditions remains the central difficulty of this subject, essentially for the reason that free streamlines may occur, separating fluid masses of different potential vorticity. The physical arguments used by Gill (1977) to close the problem discussed by him (flow from one reservoir into another) amount to an appeal to geostrophic adjustment as the mechanism controlling the geometry of the free streamline. A similar heuristic argument suggests itself in the present case.

Suppose that two particles at the boundary between the intruding and local water masses start together from rest, and are spun up to some velocity by pressure and Coriolis forces, as in geostrophic adjustment problems. Their velocity will then be the same, so that not only the pressure but also the velocity will be continuous across the boundary streamline. The matching of *both* these variables, together with other constraints on the flow, provides enough equations to calculate the streamline pattern, including the shape of the free boundary. Note that matching of h and q is different from certain free streamline boundary conditions frequently used in aerodynamics, those in which the free streamline is taken to be a vortex sheet (velocity discontinuity). A vortex sheet idealizes vorticity shed by a thin boundary layer at the point of separation. In the present problem no source of large concentrated vorticity suggests itself. Correspondingly, the observations quoted above show no local maximum of the vorticity between the two water masses in contact, the velocity distribution being quite smooth. At a minimum, continuity of velocity is an accurate prescription from a diagnostic point of view.

Anderson and Moore (1979) used the different boundary condition, $q = 0$, $h = H = B/\epsilon g$ = constant, on the free streamline along the right-hand side of the intruding jet (looking downstream). This constitutes a special case in which there is no interaction between the intruding fluid and the fluid to its side (which is of variable potential

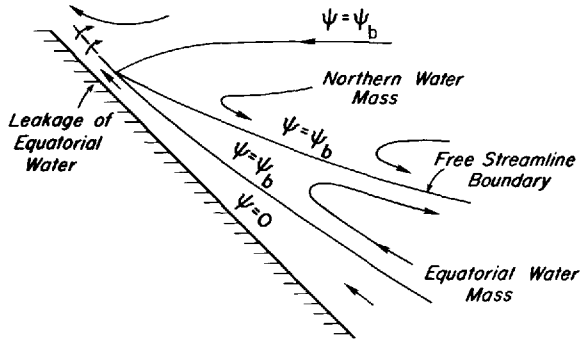

Figure 7. Schematic illustration of boundary conditions imposed, and the flow field which arises in consequence. Leakage of equatorial fluid postulated in the amount $T = \psi_b$ is accommodated between the coast ($\psi = 0$ streamline) and the innermost branch of a complex $\psi = \psi_b$ streamline. The next branch separates northern from equatorial fluid: this is the free streamline boundary along which continuity of surface layer depth and velocity are prescribed. Yet another $\psi = \psi_b$ branch arises, containing that part of the northern water mass which feeds the southeastward flow along the free streamline boundary. North of this last branch the northern fluid (which drifts slowly westward everywhere in the interior) forms a northwestward flowing boundary current, which merges with the leaking equatorial water.

vorticity, f/H). Beyond a certain latitude the equations of motion and continuity cannot be satisfied: this is interpreted as indicating a separation of the intruding jet from the coast, with the left-hand edge at zero top-layer depth, i.e., light fluid absent at a higher latitude. Because the presence or absence of light fluid is the outcome of various thermodynamic processes independent of the equations used to describe the flow, the coincidence of jet separation latitude with the absence of light fluid again amounts to a special situation.

In the present approach two water masses, each of given constant potential vorticity, are postulated to be present, and the depth and velocity are taken to be continuous across their boundary, however constituted. In a closed basin, these conditions would be sufficient to close the problem. However, in a free jet problem it is also necessary to prescribe a boundary condition at infinity in the ambient fluid, and something analogous to the discharge of a jet issuing from an orifice. In the present case it is sufficient to postulate finite velocity at infinity, and to prescribe the value of the streamfunction on the boundary streamline. Figure 7 shows schematically the flow field so envisaged (admittedly with some posterior help from calculated solutions) and the boundary conditions. Formally, these may be written as:

$$\begin{aligned} &\psi = 0 && \text{(coast)} \\ &\psi \equiv \psi_b = T = \text{constant}, h, q \text{ continuous} && \text{(free streamline boundary)}. \end{aligned} \tag{6}$$

A strictly inviscid, inertial jet in steady flow does not penetrate beyond some limiting latitude, so that $T = 0$ would be the only permissible boundary condition for the free

streamline. However, gain or loss of energy or smoothing out of the potential vorticity anomaly is likely to affect at least the high speed part of the flow, so that "leakage" along the coast may very well occur, as schematically suggested in Figure 7. Fluid of modified energy and potential vorticity is supposed to escape at the northwest corner of the equatorial water mass, while the intact part of the jet retroflects and flows back along the free streamline boundary. This conceptual model is suggested by the observational evidence: it remains to be seen whether it can be reconciled with the conservation laws written down above.

4. Parallel flow model

The observational evidence shows that the streamlines of the intruding flow, the return flow of the equatorial water mass, and the southeastward flow of the northern water mass are all, in a first approximation, parallel to the coast. This suggests that a simple parallel flow model be examined first, subject to:[2]

$$\theta \simeq \pi - \phi = \text{constant} \tag{7}$$

In this case, using Cartesian coordinates indicated in Figure 5:

$$\begin{aligned} q &\simeq |v| \\ \zeta &= \frac{\partial v}{\partial x} \\ B &= \epsilon g h + \frac{1}{2} v^2. \end{aligned} \tag{8}$$

Supposing $F = 0$ in Eqs. (5), both the Bernoulli function and the potential vorticity are conserved along streamlines. The third Eq. (5) also exposes the limitations of the parallel flow model: Eq. (7) can only be satisfied if the transport hv varies slowly enough along a streamline. This will have to be verified à posteriori.

The potential vorticity of the intruding water mass vanishes by hypothesis, while that of the northern water mass is a positive constant P:

$$\begin{aligned} \zeta &= -f \qquad \text{(equatorial)} \\ \frac{f+\zeta}{h} &= P \qquad \text{(northern).} \end{aligned} \tag{9}$$

For both water masses in parallel flow, the third of Eqs. (3), with (7), also implies the geostrophic relationship:

$$\frac{\partial h}{\partial x} = f \frac{v}{\epsilon g}. \tag{10}$$

2. The parallel flow model may be thought of as the first step in a relaxation method approach, which is to yield an approximate streamline pattern.

Eqs. (1), (8), and (9) are now readily integrated to yield the velocity distribution in the intruding equatorial water mass, while the layer depth follows from the Bernoulli equation:

$$v = \frac{f_m^2}{2\beta} - \frac{f^2}{2\beta}$$
$$h = H - \frac{v^2}{2\epsilon g} \qquad \text{(equatorial)} \tag{11}$$

where $\epsilon gH = B$, with H the "rest depth" of the equatorial water mass, and f_m is an integration constant. These equations give v and h as functions of f (related to x by Eq. 1) at a given cross-section y = constant. With H supposed constant, the only y-dependent quantity is f_m, the locus of vanishing velocity, where also $h = H$.

For the northern water mass, elimination of h from (9) and (10), results in the differential equation:

$$\frac{\partial^2 v}{\partial f^2} - \frac{P}{\epsilon g \beta^2} f v = -\frac{1}{\beta} \qquad \text{(northern)}. \tag{12}$$

As in Eq. (11), the cross-stream distance variable has been replaced by f, from Eq. (1). The solutions of Eq. (12) are the Airy functions $Ai(\eta)$, $Bi(\eta)$, and $Gi(\eta)$, with η = const. f, see Abramowitz and Stegun (1964). Once a solution for v is found, layer depth can be determined from the second of Eqs. (9).

In the northern water mass, the boundary condition at infinity is that v remains finite: the Airy function $Bi(\eta)$ may then be dropped from the homogeneous part of the solution. One integration constant remains in the solution of Eq. (12), as in (11). Matching velocity and depth at some $f = f_b$ yields two equations for the determination of these constants. Because f_b is unknown, a further condition is needed: this is provided by the second Eq. (6), which specifies the net northwestward transport of the equatorial water mass. The value of this "leakage" parameterizes processes otherwise neglected in the inviscid fluid model.

5. Calculated results

For the purpose of calculating solutions to the above equations the variables involved are conveniently made nondimensional. The scales chosen are listed in Table 1, which also gives typical values (representative of the NBCC) of these scales. The nondimensional equations are:

$$\text{(equatorial)} \qquad v = \frac{f_m^2}{2\beta} - \frac{f^2}{2\beta}$$
$$h = 1 - \frac{v^2}{2} \tag{13}$$

$$\text{(northern)} \qquad \frac{\partial^2 v}{\partial f^2} - \frac{P}{\beta^2} fv = -\frac{1}{\beta} \qquad h = P^{-1}\left(f + \frac{\partial v}{\beta \partial f}\right). \tag{14}$$

The solution of the Airy equation is:

$$v = \frac{\pi \beta^{1/3}}{P^{2/3}} Gi(\eta) + C\, Ai(\eta)$$

where

$$\eta = \frac{P^{1/3}}{\beta^{2/3}} f \tag{15}$$

and C is an integration constant. Matching of the two solutions at some $f = f_b$ (boundary latitude) yields:

$$\frac{f_m^2}{f\beta} - \frac{f_b^2}{2\beta} = \frac{\pi \beta^{1/3}}{P^{2/3}} Gi(\eta_b) + CAi(\eta_b)$$

$$1 - \frac{1}{2}\left[\frac{\pi \beta^{1/3}}{P^{2/3}} Gi(\eta_b) + CAi(\eta_b)\right]^2 = P^{-1}\left[f_b + \frac{\pi}{P^{1/3}\beta^{4/3}} Gi'(\eta_b) + \frac{P^{1/3}}{\beta^{5/3}} CAi'(\eta_b)\right]. \tag{16}$$

The second of these equations shows C to be a function of boundary latitude f_b only. Therefore the flow of the northern water mass along the boundary is the same, at given f_b, independently of what the equatorial water mass does between the coast and the boundary streamline. Furthermore, as the first of Eqs. (16) shows, the return flow leg

Table 1. Scales and typical values used in calculations.

Variable	Scale	Typical value
layer depth h	rest depth of equatorial water mass H	160 m
velocity v	Kelvin wave speed $\sqrt{\epsilon g H}$	2 m s^{-1} ($\epsilon g = 2.5 \times 10^{-2}$ m s^{-2})
Coriolis parameter f	chosen f_s	10^{-5} s^{-1}
$\beta_c = \partial f / R\partial\lambda$	$f_s^2 / \sqrt{\epsilon g H}$	5×10^{-11} m^{-1} s^{-1}
Horizontal distance x	$f_s^{-1}\sqrt{\epsilon g H}$	200 km
Potential vorticity P	f_s / H	6.25×10^{-8} m^{-1} s^{-1}
Streamfunction (transport) ψ, (T)	$\frac{\epsilon g H^2}{f_s}$	64×10^6 m^3 s^{-1}

of the equatorial water mass circulation is fixed for given f_b: with f_m determined, the velocity and layer depth distribution between f_m and f_b are fully specified.

The only unknown (at given f_b) is f_o: this follows from the specified net northward transport of equatorial water,

$$T = \beta^{-1} \int_{f_o}^{f_b} hvdf = \frac{1}{2\beta^2}\left[\left(f_b - f_o\right)\left(f_m^2 - \frac{f_m^6}{8\beta^2}\right)\right.$$
$$+ \left(f_b^3 - f_o^3\right)\left(\frac{f_m^4}{8\beta^2} - \frac{1}{3}\right) - \frac{3f_m^2}{40\beta^2}\left(f_b^5 - f_o^5\right)$$
$$\left. + \frac{1}{56\beta^2}\left(f_b^7 - f_o^7\right)\right]. \tag{17}$$

Once f_o is determined from this equation any other flow variable may be calculated. The results depend on just three nondimensional parameters, P, β, and T, entering Eqs. (13) to (17). Values appropriate to the NBCC, as observed by Flagg and McDowell (1984), are:

$$P = 4.8$$
$$\beta = 0.34 \tag{18}$$
$$T = 0.15$$

Cross-section D of Flagg and McDowell was located approximately at $f_o = 1.25$ in nondimensional units. The distributions of depth and velocity, calculated from Eqs. (13) to (17) for this section, are shown in Figure 8. Some key features of these distributions (e.g., the maximum depth) were inputs to the model, but others may be compared with observation: these are listed in Table 2. The maximum observed northwestward velocity listed is what was determined by a velocity profiler: the maximum geostrophic velocity given by the observed pycnocline slope (supposing a stagnant lower layer) was less, about 1.2 m s^{-1}. The maximum southeastward velocity was not directly observed, the value shown in the table being the geostrophic velocity. The observed transport estimates are as given by Flagg and McDowell; the calculated transports are estimates from the formula:

$$T_{12} = \int_{x_1}^{x_2} hvdx \simeq \frac{h_2^2 - h_1^2}{2f_a} \tag{19}$$

which is readily derived from Eq. (10), with f_a an appropriate averaged value of the Coriolis parameter between x_1 and x_2. Given the small ranges of f involved, a value for f_a is easily estimated. The depth was printed out in the course of the calculations. Viewed as a diagnostic tool, the parallel flow model clearly performs as well as may be expected, given the drastic idealizations on which it is based.

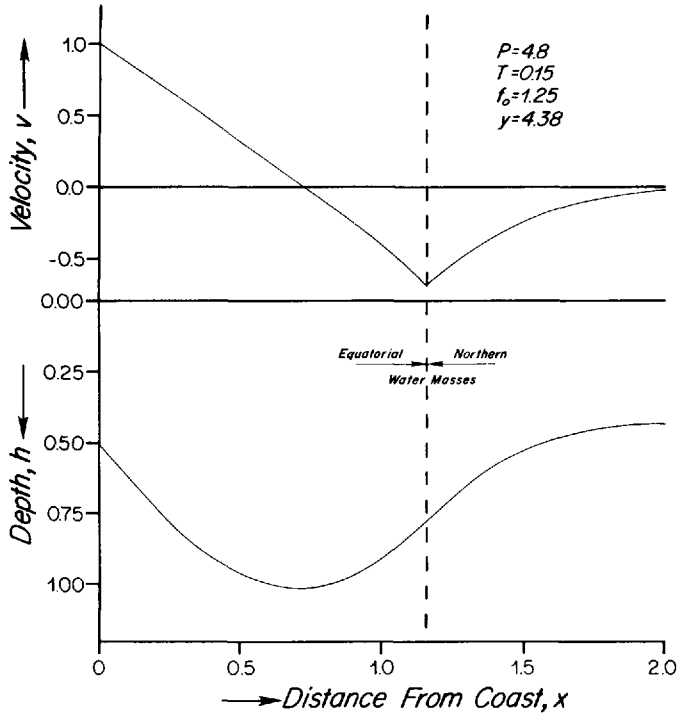

Figure 8. Distribution of velocity and depth of surface layer in a transect modeling section D of Flagg and McDowell, Figure 1 above.

6. Motion of the northern fluid mass

What does the parallel flow model imply about the large scale pattern of circulation? Consider first the flow of the northern water mass. The section at $f_o = 1.25$ showed a boundary layer of some 100 km width along the free streamline boundary within which the southeastward velocity of northern fluid was appreciable. Far from the boundary, however, the northern fluid drifts westward: asymptotically, as

Table 2. Comparison of theory at $f_o = 1.25$ with observations at Section D.

	Theory	Observation
Maximum northwestward jet velocity, m s^{-1}	2.0	> 1.50
Width of northwestward flow, km	110	150
Maximum southeastward velocity, m s^{-1}	1.36	1.1
Distance to boundary streamline, km	200	200
Width of jet in northern water mass, km	80	100
Northwestward transport of equat. water, 10^6 m^3 s^{-1}	18	16.5
Total southeastward transport 10^6 m^3 s^{-1}	16	15

$CAi(\eta) \to 0$ with increasing η, the velocity is given by the asymptotic value of $Gi(\eta)$. This is $\pi^{-1}\eta^{-1}$, so that

$$v \simeq \frac{\beta}{Pf} \qquad (f \to \infty). \tag{20}$$

The result equals the projection to the shore-parallel direction of the asymptotic quasi-geostrophic westward drift in a surface layer of constant potential vorticity:

$$u_z = -\frac{\beta_c}{Pf} \tag{21}$$

where u_z is zonal velocity, and β_c "conventional" β, see Eq. (1).

From the relationship between the Bernoulli function and potential vorticity (second of Eqs. 5) it follows that in the northern water mass:

$$h + \frac{v^2}{2} = P\psi + \text{const.} \tag{22}$$

Along the boundary streamline, on account of the postulated continuity of depth and velocity, the value of the Bernoulli function is H, the rest-depth of the equatorial water mass, which is the chosen depth scale. Hence the transport between the boundary and an arbitrary streamline within the northern water mass is, in nondimensional units:

$$\psi - \psi_b = \frac{1}{P}(h + \frac{v^2}{2} - 1). \tag{23}$$

Proceeding along a normal to the streamlines from the free streamline boundary northward, the value of ψ at first decreases, as both h and v^2 decrease in the northeastward flowing boundary layer. Farther away, however, the velocity becomes small, and the variation of the Bernoulli function comes to be dominated by the increase of layer depth with increasing latitude, which constant potential vorticity implies. Thus the streamfunction increases again, eventually back to the boundary streamline value, which is approximately given by:

$$\begin{aligned} h &\simeq 1 \\ f &\simeq P. \end{aligned} \qquad (\psi = \psi_b) \tag{24}$$

Thus between the latitude $f \simeq P$ and the free streamline boundary a semi-closed circulation loop is present, the westward drift of the northern water mass being conducted away by the southeastward flow in the free streamline boundary layer. Where the northern (zonal) branch of the $\psi = \psi_b$ streamline meets the free streamline, an internal stagnation point arises, characterized by

$$\begin{aligned} v_b &= 0 \\ h_b &= H. \end{aligned} \tag{25}$$

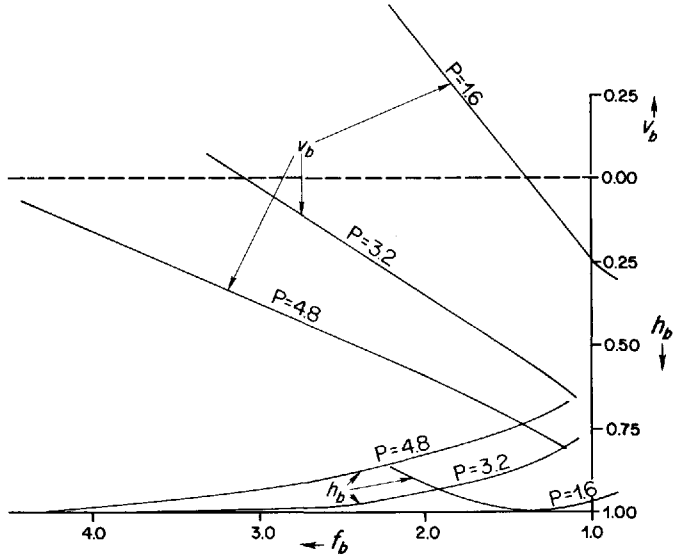

Figure 9. Velocity v_b and layer depth h_b along the free streamline boundary, for various values of P, as functions of f_b.

The location of this stagnation point may be discovered by solving Eq. (16) for vanishing v_b, or

$$\frac{\pi}{P^{1/3}\beta^{4/3}} Gi'(\eta_b) + \frac{P^{1/3}}{\beta^{5/3}} CA_i'(\eta_b) = P - f_b$$
$$CAi(\eta_b) = -\frac{\pi \beta^{1/3}}{P^{2/3}} Gi(\eta_b). \tag{26}$$

The solution, $f_b = f_s$, is a function only of P and β; it is generally somewhat less than the latitude ($f \approx P$) of the northern branch of the streamline $\psi = \psi_b$.

North of the stagnation point, the flow of northern fluid along the free streamline boundary is northwestward. Figure 9 shows the variation of the boundary velocity and depth for different values of P, two of the curves extending past a stagnation point.

7. Behavior of the intruding water mass

According to the analysis above, the flow in the return leg of the equatorial water mass is also independent of the net northwestward transport, much as the flow of the northern fluid. The southwestward transport of equatorial fluid on the south side of the free streamline increases with decreasing f_b from zero at the stagnation point. Variations of potential vorticity of the northern water mass have a controlling influence on the return flow of equatorial fluid. At a boundary latitude around f_b = 1.95, for example, the return flow in dimensional units varies from 16×10^6 m^3 s^{-1} to

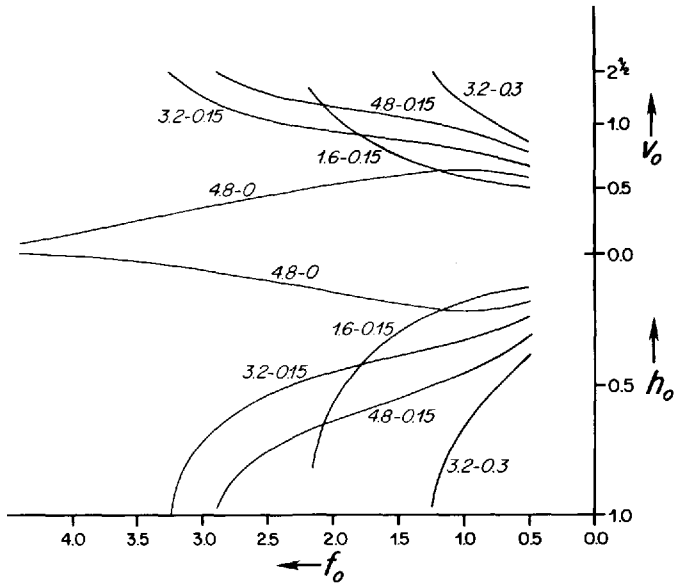

Figure 10. Velocity v_o and layer depth h_o at the coast for various $P - T$ combinations noted on the curves, as functions of coastal latitude f_o.

12×10^6 m^3 s^{-1} to 0.5×10^6 m^3 s^{-1} for the three values of $P = 4.8$, 3.2, 1.6, for which calculations have been made. The qualitative result is already implicit in the distribution of velocity along the boundary streamline: there can be little transport if this, maximum, velocity of southeastward flow is low. As these results show, at the two higher values of the potential vorticity quoted ($P = 4.8$, 3.2) the southeastward flow increases streamwise and carries transport in the vicinity of the scale latitude $f_b = 1$ (4N) comparable to the observed transport of the NECC. However, near the northern limit of the calculations the southeastward transport is small in the case characterized by $P = 4.8$ (order 10^6 m^3 s^{-1}). With $P = 3.2$ a stagnation point occurs on the boundary streamline, so that near the northern limit, the flow becomes northwestward everywhere.

A clear northern limit of the parallel flow model was always reached in these calculations: beyond a certain coast latitude f_o, depending on T and P, no roots could be found for Eq. (17). Near this limit the coastal velocity v_o generally increased and the depth h_o decreased rapidly, approaching the limit set by a surfacing of the pycnocline. Figure 10 shows the variation of h_o, v_o along the coast for the cases examined. In two of these cases the flow had passed the stagnation point on the free streamline, by the time the limit of the parallel flow model was reached. In two other cases the flow apparently choked up before the stagnation point on the free streamline, although in the case closely simulating the observed flow profiles ($P = 4.8$, $T = 0.15$) not too far from where the stagnation point would be expected to occur.

The choking of the flow at a given latitude, associated with a surfacing of the pycnocline, is analogous to results obtained by Charney (1955) and Anderson and Moore (1979) and may be expected to be related to the constraint embodied by Eq. (19): for given maximum depth, at a given latitude, only a certain amount of fluid can be transported by a coast-parallel jet. To examine this constraint for the zero potential vorticity case suppose that $f_m < f_b$ (so that the velocity vanishes within the equatorial water mass, i.e. there is some return flow) and calculate the transport of the northwestward flow leg alone:

$$\begin{aligned} T_m &= \beta^{-1} \int_{f_o}^{f_m} hvdf \\ &= \frac{2}{3} f_m^3 - f_m^2 f_o + \frac{f_o^3}{3} \\ &= \frac{1}{8\beta^2}\left[\frac{16}{35} f_m^7 - f_m^6 f_o + f_m^4 f_o^3 - \frac{3}{5} f_m^2 f_o^5 + \frac{1}{7} f_o^7\right]. \end{aligned} \tag{27}$$

Having in mind the seasonal variations of northward transport by the NBCC between about 0.15 and 0.50, one might ask what this equation implies for fixed T_m. It is convenient to introduce the variables:

$$\begin{aligned} w &= f_o^{-1} \beta^{-1} (f_m - f_o) = \beta^{-1} (\gamma - 1) \\ \gamma &= \frac{f_m}{f_o}. \end{aligned} \tag{28}$$

The width of the northward flow leg is $f_o w$; γ is another measure of the same variable, but is always greater than one.

Eq. (27) may be reduced after some elementary manipulations to:

$$a w^4 - \frac{b}{f_o^4} w^2 + \frac{c}{f_o^7} = 0 \tag{29}$$

where

$$\begin{aligned} a &= \frac{1}{280} (16\gamma^3 + 29\gamma^2 + 20\gamma + 5) \\ b &= \frac{1}{3} (2\gamma + 1) \\ c &= \frac{2T_m}{\beta}. \end{aligned}$$

The coefficients a, b, and c are all of order one and positive definite, as is f_o at latitudes of interest. Eq. (29), regarded as an equation for the nondimensional width of the northwestward leg of the flow, therefore has roots much as a quadratic equation

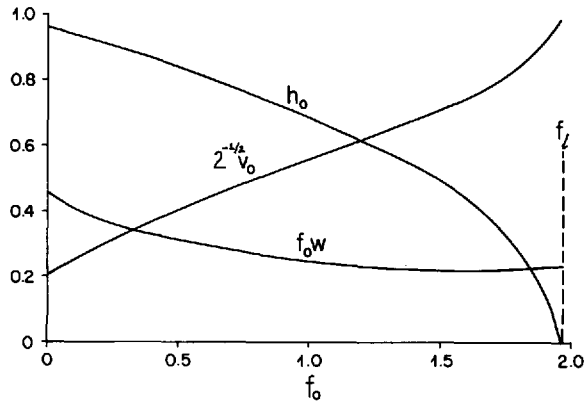

Figure 11. Layer depth h_o, and velocity v_o at the coast, and current width $f_o w$, to locus of zero velocity, for prescribed total northwestward transport $T_m = 0.3$ in function of coast latitude f_o.

with constant coefficients. One of the two roots yields an unrealistic shore depth $h_o < 0$. The other root is:

$$w^2 = \frac{b - \sqrt{b^2 - 8\, a f_o \beta^{-1} T_m}}{2\, a f_o^4}. \tag{30}$$

With w, a, b being functions of γ, this is an implicit equation for γ. It is readily solved by an iterative procedure, starting, for example, with the asymptotic values of a, b, corresponding to $\gamma = 1$, i.e., $a = 1/4$, $b = 1$. The results show what given total northwestward transport implies, in particular for the layer depth h_o, and velocity v_o, at the coast. At higher latitudes f_o the depth h_o and the width of the current w become smaller, the velocity v_o greater. An example of the behavior of the solution, for fixed $T_m = 0.3$ is shown in Figure 11. This resembles the results for fixed T shown in Figure 10.

The discriminant of Eq. (30) vanishes at a "limiting" shore-latitude:

$$f_o = \frac{\beta b^2}{8\, a T_m} \equiv f_l \tag{31}$$

where the physically realistic root merges with the root giving negative h_o, at the value:

$$w_l^2 = \frac{b}{2\, a f_l^4} = \frac{h\, T_m}{\beta b f_l^3}. \tag{32}$$

The width w_l, and corresponding shore latitude f_l may again be found by iteration. The value of f_l is the maximum shore latitude at which the equations may be satisfied

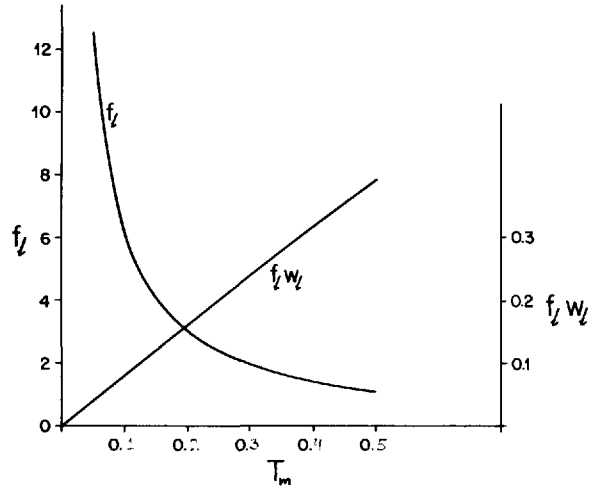

Figure 12. Limiting latitude f_l reached by a shore-parallel surface layer jet, and current width $f_l w_l$, as functions of prescribed northwestward transport T_m.

with a prescribed T_m, $f_l = f_l(T_m)$. Figure 12 shows the limiting shore-latitude and the corresponding width of the current, $f_l w_l$, as functions of the transport T_m.

From the merging of the two roots with positive and negative h_o one might expect that at $f_o = f_l$ the shore depth h_o vanishes so that

$$v_o = \sqrt{2} = \frac{f_m^2 - f_o^2}{2\beta} = \frac{f_o^2(\gamma^2 - 1)}{2\beta}. \tag{33}$$

The two criteria, Eqs. (31) and (33), are not satisfied exactly at the same shore latitude, however. If one writes for the solution of (33) $f_o = f_v$, one has

$$f_v = \frac{2\sqrt{2}\,\beta}{(\gamma^2 - 1)^{1/2}} \tag{34}$$

as against

$$f_l = \left(\frac{b}{2a}\right)^{1/4} \frac{\beta^{1/2}}{(\gamma - 1)^{1/2}} \tag{35}$$

from Eq. (32). Both are functions of γ alone, the ratio of the two solutions being

$$\frac{f_v}{f_l} = \left[\frac{16a}{(\gamma + 1)^2 b}\right]^{1/4} \tag{36}$$

which tends to unity for $\gamma \longrightarrow 1$, but is always slighty greater than one. The flow chokes because the equations of motion and continuity cannot be satisfied under the parallel flow postulate, not because the shore depth reduces to zero. The shore depth does, however, become small at this latitude, and the nondimensional velocity nearly reaches

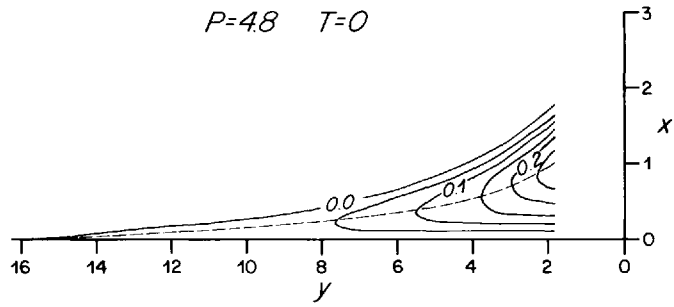

Figure 13. Streamline pattern in the intruding fluid between the coast and the free streamline for the case of zero leakage $T = 0$, $P = 4.8$. Cross-shore scale has been stretched to show detail of streamlines better: this also approximately doubles the angles.

its limit of 2, as one readily calculates for specific choices of T_m, and β. Note that this "inner" solution does not explicitly depend on the potential vorticity of the northern water mass. Such dependence is, nevertheless, implicit in the value of T_m, which is the sum of the prescribed net northwestward transport T and the southeastward return transport. The latter, as was discussed earlier in detail, depends primarily on P, given by what one might call the "outer" system.

The actual choking latitude is determined by an interplay of the inner and outer solutions. Eq. (32) yields T_m as a function of $f_o = f_l$. The outer solution, Eq. (16) yields quantities from which the southeastward transport may be determined, and Eq. (18) couples this to a specific shore latitude f_o, thus in effect yielding another $T_m(f_o)$ relationship. The two relationships for T_m are simultaneously satisfied at the choking latitude.

Of special interest is the case $T = 0$ (zero northwestward leakage). In Figure 10 this constitutes the one exception to the rule that v_o increases, h_o decreases streamwise. The northern limit is reached here at a stagnation point, where the coast and the free boundary streamline meet. The northwestward transport in this case never reaches its limiting value, the intruding jet does not choke: the streamline gradually turn offshore instead, and a semi-closed circulation loop results, see Figure 13. The one-way transport at any cross section is what is determined by the location of the free streamline boundary.

The overall streamline pattern for the case simulating the observed flow at $f_o = 1.25$ (Eq. 18, Fig. 8, and Table 2) is shown in Figure 14. At a coast latitute $f_o \simeq 2.89$ the flow chokes as the prescribed net transport T comes to equal the maximum possible northwestward transport T_m.

8. Validity of parallel flow model

How valid is the approximation underlying the parallel flow model, Eq. (7), or stated in another way, how close do the calculated streamline patterns come to satisfying the full equations (5a)? The most obvious discrepancy evident in Figure 14 is the

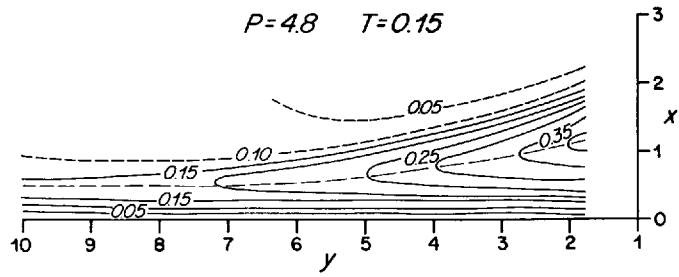

Figure 14. Streamline pattern for leakage $T = 0.15$, $P = 4.8$ about characteristic of the NBCC, also showing two streamlines in the northern fluid (---) near the free streamline boundary, and the $f = f_m$ locus (--) in the intruding fluid. Scale distortion as in previous illustration.

cross-shore flow along the $f = f_m$ locus, where the alongshore flow component vanishes. Along this locus, the typical magnitude of the cross-shore velocity is 0.1 m s^{-1}, of the velocity gradient $\partial q/\partial n \equiv hq\ (\partial q/\partial \psi)\ 10^{-7}\ s^{-1}$, two orders of magnitude less than f. The second of Eqs. (5a) then has to be satisfied by an appropriately small radius of curvature for the streamlines:

$$\frac{\partial \theta^{-1}}{\partial s} = -\frac{q}{f} = \text{order 10 km.}$$

As calculated from the parallel flow model, the retroflecting streamlines would exhibit sharp corners along the $f = f_m$ locus. In the illustrations they have already been shown rounded. A more accurate relaxation calculation would presumably also push the streamlines apart by order 10 km, to accommodate the turning flow. On the scale of the entire intrusion pattern this is only a small modification, and hardly worth a second round of calculations.

Of greater potential impact is the third of Eqs. (5), which predicts divergence of streamlines where the transport hq decreases in the streamwise direction. This is an equation for the radius of curvature of the *normal* to the streamlines:

$$r \equiv \left(\frac{\partial \theta}{\partial n}\right)^{-1} = hq\left[\frac{\partial}{\partial s}(hq)\right]^{-1}. \tag{37}$$

The product hq vanishes with either h or q, and in the equatorial water mass it varies with one of its constituents, say q, as:

$$hq = q - \frac{q^3}{2}. \tag{38}$$

This has a maximum at $q^2 = 2/3$, when also $h = 2/3$, or $q = \sqrt{h}$, the internal wave propagation velocity at the local depth. Proceeding with the flow along a streamline, if h decreases monotonically from a value near unity, the velocity q and transport hq both increase at first. However, when the depth drops to a value below $2/3$, the transport

begins to decrease even though the velocity increases further. In analogy with compressible flow or channel flow one might call the condition supercritical: the velocity is faster than the local wave propagation velocity. The decrease in transport requires a divergence of the streamlines, in analogy with the widening of the Laval nozzle downstream of the throat. The question in the present context is, how rapid is the widening—or the convergence prior to reaching critical velocity.

In some of the examples shown above the shore velocity increased well beyond the critical value of $(\frac{2}{3})^{1/2} = 0.8165$. The shore value of the radius of curvature r, defined by Eq. (37), may be calculated from the parallel flow model using Eq. (13):

$$r = \tan\phi \left(f_m \frac{\partial f_m}{\partial f_o} - f_o \right) \left[1 - \frac{3}{2} \left(\frac{f_m^2 - f_o^2}{2\beta} \right)^2 \right]. \tag{39}$$

Close to the choking latitude, $f_o = 2.865$, of the diagnostic case, $P = 4.8$, $T = 0.15$, the radius of curvature, calculated from this equation was 0.4, from which one estimates a maximum angular deflection (along the $hq = |\, hq \,|_{max} = 0.44$ streamline) of less than 10°. The parallel flow model therefore remains a good approximation right up to the choking latitude.

Guided by the compressible flow analogy, one would surmise that a shock wave (internal hydraulic jump) develops at the choking latitude, where some of the energy of the flow is dissipated. Because there is little or no experimental evidence on the shape of any such shocks in the oceanic context, the matter will not be pursued further: the "leakage" of equatorial fluid past the choking latitude will be left ascribed to unspecified energy dissipation and potential vorticity homogenization processes.

9. Discussion

The steady, inviscid, inertial model of the NBCC developed above is clearly overidealized and its predictions must be interpreted with caution. Because the flow chokes at some high enough latitude for any given leakage, the only transport condition strictly compatible with the idealizations is $T = 0$, zero net northwestward transport. However, when the predicted choking latitude is high enough, say 10 or 12N, it is realistic to suppose that energy dissipation and potential vorticity homogenization modify the intruding water mass to the point where it "forgets" its origins. Northwestward leakage of equatorial fluid after an alongshore trip from the equator of 1500 km or so, is then a realistic hypothesis. One might also expect strong eddies to develop as the choking latitude is approached, in accord with the observations discussed by Bruce (1984).

Similarly, the abrupt change of potential vorticity across the free streamline separating northern from equatorial fluid suggests hydrodynamic instability and the likelihood of eddy formation. With these qualifications, the model shows that the massive seasonal retroflection of the NBCC is readily understood as an inertial

phenomenon, due essentially to the difference in potential vorticity between the local and intruding water masses. The key control variable is the nondimensional potential vorticity P of the northern mass. With the scaling used, this is simply the ratio of rest depths at the scaling latitude of 4N, of equatorial to northern mass. One surmises that as the trade winds pile up equatorial water near the coast, the rest-depth increases until the water mass arriving from the east can escape within the NBCC.

The moderate upwelling at the coast, reported in observational studies, is consistent with the slow surfacing of the pycnocline that accompanies the northwestward flow with limited leakage (perhaps somewhat less than the 10×10^6 m^3 s^{-1} supposed in the calculations). The reported eddy activity is consistent with the notion of instability, both near the choking latitude and along the boundary streamline. The characteristic size of these eddies should be proportional to the local radius of deformation, and hence decrease as f^{-1}, again in accord with observations.

Within its clear limitations, the theoretical model accounts quite well for the observed and inferred behavior of the surface NBCC. From a theoretical point of view the most significant conclusion one can draw from the model is perhaps that the free streamline boundary condition adopted above was a realistic idealization. This opens up the possibility of applying the same idealization to other problems involving western boundary currents.

Acknowledgments. This work was supported by the Office of Naval Research under Contract No. N00014-82-C-0019, NR 083-004. I have profited from many discussions with Dr. Charles Flagg. Mr. J. H. Churchill carried out the calculations resulting in Figures 8 to 14. Contribution number 5702 of the Woods Hole Oceanographic Institution.

REFERENCES

Abramowitz, M. and I. A. Stegun. 1964. Handbook of Mathematical Functions, National Bureau of Standards, Washington, 1046 pp.

Anderson, D. L. T. and D. W. Moore. 1979. Cross-equatorial inertial jets with special reference to very remote forcing of the Somali Current. Deep-Sea Res., *26A,* 1–22.

Birkhoff, G. and E. H. Zarantonello. 1957. Jets, Wakes and Cavities, Academic Press, N.Y.

Borstad, G. A. 1982. The influence of the meandering Guiana Current and Amazon River discharge on surface salinity near Barbados. J. Mar. Res., *40,* 421–434.

Bruce, J. G. 1984. Comparison of eddies off the North Brazilian and Somali coasts. J. Phys. Oceanogr., *14,* 825–832.

Charney, J. G. 1955. The Gulf Stream as an inertial boundary layer. Proc. Nat. Acad. Sci. USA, *41,* 731–740.

Cochrane, J. D. 1969. Low sea surface salinity off northeastern South America in summer 1964. J . Mar. Res., *27,* 327–334.

Csanady, G. T. 1984. Warm water mass formation. J. Phys. Oceanogr., *14,* 264–275.

Flagg, C. N. and S. McDowell. 1984. Hydrographic and current observations on the continental slope and shelf of the Western Equatorial Atlantic, (unpubl. ms.).

Froehlich, P. N., D. K. Atwood and G. S. Giese. 1978. Influence of Amazon River discharge on surface salinity and dissolved silicate concentration in the Caribbean Sea. Deep-Sea Res., *25,* 735–744.

Gibbs, R. J. 1980. Wind-controlled coastal upwelling in the western equatorial Atlantic. Deep-Sea Res., *27A,* 857–866.

Gill, A. E. 1977. The hydraulics of rotating channel flow. J. Fluid Mech., *80,* 641–671.

Hurlburt, E. M. and N. Corwin. 1969. Influence of the Amazon River outflow on the ecology of the Western Tropical Atlantic. J. Mar. Res., *27,* 55–72.

Kidd, R. and F. Sander. 1979. Influence of Amazon River discharge on the marine production system off Barbados, West Indies. J. Mar. Res., *37,* 669–681.

Metcalf, W. G. 1968. Shallow currents along the northeastern coast of South America. J. Mar. Res., *26,* 232–243.

Metcalf, W. G. and M. C. Stalcup. 1967. Origin of the Atlantic Equatorial Undercurrent. J. Geophys. Res., *72,* 4959–4975.

Molinari, R. L. 1983. Observations of near-surface currents and temperature in the central and western tropical Atlantic Ocean. J. Geophys. Res., *88,* 4433–4438.

Philander, G. and W. Düing. 1979. The oceanic circulation of the tropical Atlantic, and its variability, as observed during GATE. Deep-Sea Res., GATE suppl. *2,* 1–27.

Richardson, P. L. and T. K. McKee. 1984. Average seasonal variation of the Atlantic North Equatorial Countercurrent from ship drift data. J. Phys. Oceanogr., *14,* 1226–1238.

Ryther, J. H., D. W. Menzel and N. Corwin. 1967. Influence of the Amazon River outflow on the ecology of the western tropical Atlantic, I: Hydrography and nutrient chemistry. J. Mar. Res., *25,* 69–83.

Shen, C. Y. 1981. The rotating hydraulics of the open-channel flow balance between two basins. J. Fluid Mech., *112,* 161–188.

Steven, D. M. and A. L. Brooks. 1972. Identification of Amazon River water at Barbados, West Indies, by salinity and silicate measurements. Mar. Biol., *14,* 345–348.

Woods, L. C. 1961. The Theory of Subsonic Plane Flow. Cambridge Univ. Press, 594 pp.

Received: *22 May, 1984;* revised: *22 May, 1985.*